Chalkophore mediated respiratory oxidase flexibility controls *M. tuberculosis* virulence

John A. Buglino[1,*], Yaprak Ozakman[1,*], Chad Hatch[2], Anna Benjamin[1], Derek Tan[2,3], Michael S. Glickman[1,#]

1-Immunology Program, Sloan Kettering Institute
2-Chemical Biology Program, Sloan Kettering Institute
3-Tri-Institutional Research Program
Memorial Sloan Kettering Cancer Center, 1275 York Avenue, New York, New York 10065 USA

*Equal contribution

#Correspondence:
glickmam@mskcc.org
1275 York Ave
New York, NY 10065
646-888-2368

Summary

Oxidative phosphorylation has emerged as a critical therapeutic vulnerability of *M. tuberculosis*, but it is unknown how *M. tuberculosis* and other pathogens maintain respiration during infection. *M. tuberculosis* synthesizes diisonitrile lipopeptide chalkophores that chelate copper tightly, but their role in host-pathogen interactions is also unknown. We demonstrate that *M. tuberculosis* chalkophores maintain the function of the heme-copper *bcc:aa*$_3$ respiratory oxidase under copper limitation. Chalkophore deficient *M. tuberculosis* cannot survive, respire to oxygen, or produce ATP under copper deprivation in culture. *M. tuberculosis* lacking chalkophore biosynthesis is attenuated in mice, a phenotype that is severely exacerbated by loss of the CytBD alternative respiratory oxidase (encoded by *cydAB*), revealing a multilayered flexibility of the respiratory chain that maintains oxidative phosphorylation during infection. Taken together, these data demonstrate that chalkophores counter host inflicted copper deprivation and highlight that protection of cellular respiration is a critical virulence function in *M. tuberculosis*.

Introduction

Bacterial pathogens are subjected to diverse stresses imposed by host immunity and deploy countermeasures to neutralize immune effectors. The ubiquity of metalloenzymes in all bacteria necessitates acquisition of trace metals such as iron, zinc and manganese, a vulnerability that is exploited by host nutritional immunity, which limits these metals (1). To counter this metal limitation by the host, pathogens deploy diverse high affinity metal acquisition systems including siderophores for iron and zinc (2-4), and transporters and metallophores for zinc and manganese (1, 3, 5-7). In addition to metal limitation, the host also deploys metals as antimicrobial effectors to kill bacteria (8). Copper and zinc are deposited into the phagosome of infected macrophages as antimicrobials and pathogens employ metal resistance systems such as metal efflux transporters (9-11) and metal binding proteins controlled by metal dependent repressors (9-11). Although both metal limitation and metal intoxication limit pathogen growth, in most cases the essential bacterial metalloenzymes rendered dysfunctional by nutritional immunity are incompletely defined.

M. tuberculosis is a successful global pathogen that can survive in both macrophages and neutrophils. *M. tuberculosis* experiences both high copper (10-15) and high zinc (12) in the macrophage phagosome and resists metal toxicity through several mechanisms including efflux and metal chelation. Recent data also indicates that *M. tuberculosis* experiences zinc starvation during infection, possibly imposed by calprotectin in caseum (16). However, it is unknown whether copper acquisition, and resistance to copper deprivation, are part of the virulence program of *M. tuberculosis*. *M. tuberculosis* synthesizes diisonitrile lipopeptide natural products directed by the 5 gene *nrp* operon, present in *M. tuberculosis* and *M. marinum*, but not nonpathogenic mycobacteria (17-20). The *nrp* operon is induced by copper deprivation and growth of *M. tuberculosis* lacking diisonitrile lipopeptide biosynthesis is inhibited in copper limiting conditions (21), establishing diisonitrile lipopeptides as mycobacterial chalkophores. However, the role of diisonitrile chalkophores in *M. tuberculosis* pathogenesis is not understood, including whether copper deprivation is imposed by the host during infection, and the specific bacterial pathways that require copper supplied by the chalkophores. In this study, we demonstrate that diisonitrile chalkophores supply copper to the heme-copper respiratory oxidase to maintain respiration and ATP production. The heme-copper oxidase of chalkophore deficient *M. tuberculosis* is compromised by the host during infection, but *M. tuberculosis* compensates with the heme-dependent cytochrome BD (CytBD). *M. tuberculosis* lacking

71 diisonitrile chalkophore biosynthesis and CytBD is severely attenuated, demonstrating that this
72 multilayered system for protecting respiration is a critical virulence function of *M. tuberculosis*.

Results

Chalkophore deficient *M. tuberculosis* upregulates respiratory chain components in response to copper deprivation

To understand the function of diisonitrile chalkophores in *M. tuberculosis*, we examined the transcriptional profile of wild type (WT) and Δ*nrp M. tuberculosis* treated with 10 μM tetrathiomolybdate (TTM), a copper chelator previously shown to inhibit the growth of *M tuberculosis* lacking chalkophore biosynthesis (21). Copper chelation had relatively few effects on gene expression in wild type *M. tuberculosis* (Figure 1A, Table S3). In contrast, in Δ*nrp M. tuberculosis* we observed upregulation of the genes of the chalkophore cluster (other than *nrp* itself) at baseline, consistent with prior data demonstrating autoregulation (21). In addition, a cluster of genes was induced by copper deprivation in Δ*nrp* cells, but not wild type cells, encoding components of the respiratory chain, including *cydABDC* (encoding components of the heme dependent oxidase CytBD), *qcrABC* (encoding subunits of the *bcc:aa*$_3$ heme-copper oxidase), and subunits of ATP synthase (Fig 1A). Prior work demonstrated that genetic or pharmacologic disruption of the *bcc:aa*$_3$ respiratory oxidase, including by Q203, an inhibitor of the QcrB subunit of the *bcc:aa*$_3$ oxidase, transcriptionally upregulates genes encoding components of the respiratory chain, including *cydAB* and ATP synthase (22, 23). Treatment of wild type and Δ*nrp* with Q203 reproduced the published pattern in wild type cells and indicated that diisonitrile chalkophore deficient cells still respond to Q203 (Figure 1). To confirm the RNA sequencing results, we quantitated the transcript encoding the *cydA* encoded subunit of the CytBD oxidase with different concentrations of TTM and observed no induction at any TTM concentration in wild type cells, but progressive induction of CydA with escalating TTM concentrations in the Δ*nrp* strain (Figure 1B). Longer durations of copper deprivation induced *cydA* in both wild type and Δ*nrp*, with higher induction in Δ*nrp* (Figure 1C). Escalating concentrations of TTM did not affect wild type *M. tuberculosis* growth but caused a graded inhibition of growth of the Δ*nrp* strain in liquid media (Fig 1D). These data indicate that copper deprivation in *M. tuberculosis* lacking diisonitrile chalkophore biosynthesis stimulates gene expression that mimics inhibition of the *bcc:aa*$_3$ respiratory oxidase.

Chalkophores protect the *bcc:aa*$_3$ oxidase from copper deprivation

Inhibition of *bcc:aa*$_3$ oxidase by Q203 (22, 24) or other QcrB inhibitors (25-28) is bacteriostatic and incompletely inhibits respiration, but becomes bactericidal and abolishes oxidative phosphorylation in *M. tuberculosis* lacking the alternative cytochrome BD (Δ*cydAB*, (22, 28)) or

109 treated with a CytBD inhibitor (29). Although the *bcc:aa$_3$* oxidase and CytBD are functionally
110 redundant, they differ in cofactor usage for electron transfer: *bcc:aa$_3$* is a heme-copper oxidase
111 with three copper ions in the electron transport path (30-33), whereas CytBD uses heme
112 prosthetic groups but not copper (34)(Figure 2A).
113 To test whether diisonitrile chalkophores maintain the function of the copper dependent
114 *bcc:aa$_3$* oxidase under copper limitation, we generated *M. tuberculosis* Δ*nrp*Δ*cydAB*, along with
115 control strains lacking *cydAB* alone and genetically complemented strains. We tested the effect
116 of TTM on growth in liquid media and observed mild inhibition of growth of *M. tuberculosis* Δ*nrp*
117 and no effect on Δ*cydAB* (Figure 2B). However, growth of Δ*nrp*Δ*cydAB* was severely inhibited
118 by TTM, an effect that was reversed by genetic complementation with either *nrp* or *cydABDC*
119 (Figure 2B). Assays on copper chelated agar media revealed a dramatic sensitization of
120 chalkophore deficient *M. tuberculosis* by loss of the secondary oxidase with 6 logs of killing, a
121 phenotype that was also complemented by *nrp* or *cydABDC* (Figure 2C, S1). To determine
122 whether the phenotypes of Δ*nrp* are due to diisonitrile chalkophore deficiency rather than some
123 function of the genetic element independent of the diisonitrile chalkophore itself, we first
124 repeated the same *cydAB* synergy test with *M. tuberculosis* Δ*fadD10*, a second biosynthetic
125 gene in the *nrp* operon that is required for chalkophore mediated resistance to copper chelation
126 (21). Δ*fadD10*Δ*cydAB M. tuberculosis* was also dramatically sensitized to BCS
127 bathocuproinedisulfonic acid, disodium salt (BCS, another copper chelator) or TTM to a similar
128 degree as Δ*nrp*Δ*cydAB* (Figure S1B, C). To demonstrate that the copper deprivation sensitivity
129 of the Δ*nrp*Δ*cydAB* strain is due to absence of the diisonitrile lipopeptide, we synthesized an
130 analogue of a reported *M. tuberculosis* diisonitrile chalkophore (20) having 4-carbon side chains
131 (see Methods and SI Appendix). This C4 L-ornithyl-L-phenylalaninol acetate diisonitrile (C4-Orn-
132 Phin-OAc) was synthesized via a route analogous to our previously reported syntheses of a
133 *Streptomyces* diisonitrile (35). This synthetic diisonitrile efficiently rescued Δ*nrp*Δ*cydAB* from the
134 growth inhibition imposed by TTM in liquid media (Figure 2D), consistent with direct mediation of
135 this effect by the diisonitrile lipopeptide product of the *nrp* locus.
136 The data above indicates that diisonitrile biosynthesis is necessary to resist the effects of
137 copper starvation and that one of the effects of this copper starvation is dysfunction of the
138 *bcc:aa$_3$* oxidase. To determine whether maintenance of respiratory oxidase function under
139 copper starvation is the only function of diisonitrile chalkophores, we executed genetic and
140 biochemical epistasis testing. Deleting *ctaD,* which encodes one subunit of the *bcc:aa$_3$* oxidase,
141 alone or in diisonitrile chalkophore deficient cells (Δ*nrp*Δ*ctaD*), impaired growth of *M.*

142 *tuberculosis* in copper replete media (Figure 2E), but copper deprivation had no additional
143 effect, indicating that the heme-copper oxidase complex is the only target impacted by copper
144 starvation (Figure 2E). Similarly, the growth inhibitory effect of copper starvation on Δ*nrp* cells
145 was similar in degree to treatment of WT or Δ*nrp* cells with Q203, but combined treatment was
146 not synergistic (Figure 2F), again indicating that the heme-copper oxidase is inactivated by
147 copper deprivation when the diisonitrile chalkophore is missing and that no additional targets
148 are relevant to copper deprivation-induced growth arrest.
149
150 **Chalkophores maintain oxidative phosphorylation and ATP production**
151
152 To determine whether diisonitrile chalkophores directly maintain respiration during copper
153 deprivation, as suggested by the growth and survival data above, we measured oxygen
154 consumption by *M. tuberculosis*. We first utilized a qualitative methylene blue assay of oxygen
155 consumption (22, 29). In this assay, decolorization of methylene blue in a sealed tube indicates
156 oxygen depletion, as observed in both WT or Δ*nrp*Δ*cydAB M. tuberculosis* treated with DMSO
157 (Figure 3A), indicating intact respiration in chalkophore deficient cells in basal conditions.
158 Treatment with Q203 did not impair oxygen consumption in WT cells but did in Δ*nrp*Δ*cydAB*,
159 consistent with its inhibition of the *bcc*:aa_3 oxidase (Figure 3A). Treatment of wild-type cells with
160 Q203 in combination with ND-011992, a small-molecule inhibitor of CytBD, also blocked oxygen
161 consumption, consistent with prior data (Figure S4A) (22, 29). Copper chelation with 50 μM TTM
162 had no effect on wild type cells but abolished respiration in Δ*nrp*Δ*cydAB*, indicating that copper
163 deprivation inhibits respiration through the *bcc:*aa_3 oxidase (Figure 3A). Taken together, these
164 data are consistent with a model in which *M. tuberculosis* can respire via either the *bcc*:aa_3
165 oxidase or CytBD, with the former requiring diisonitrile chalkophore-mediated copper acquisition
166 under copper starvation. The full effect of loss of chalkophore biosynthesis is masked by the
167 redundancy of the oxidases, but in cells that rely only on *bcc*:aa_3 oxidase, respiration is
168 abolished by copper deprivation.
169
170 To measure oxygen consumption more quantitatively, we adopted a spot sensor assay (36),
171 that can noninvasively measure oxygen in sealed vessels, allowing serial measurements. WT
172 *M. tuberculosis* consumed oxygen down to the lower limit of detection, and treatment with the
173 CytBD inhibitor ND-011992 (29) had no effect (Figure 3B). Treatment with the QcrB inhibitor
174 Q203 delayed but did not prevent oxygen consumption, consistent with the methylene blue
175 results and prior data (22, 24, 29). However, treatment with the combination of Q203 and ND-
176 011992 completely inhibited oxygen consumption (Figure 3B). Applying this assay to diisonitrile

177 chalkophore deficient strains, we observed that copper deprivation delayed but did not prevent
178 respiration in Δ*nrp* cells (Figure 3C), consistent with compensation by CytBD, but abolished
179 respiration in Δ*nrp*Δ*cydAB* cells, a phenotype that was rescued by genetic complementation with
180 the *nrp* gene (Figure 3D). To confirm that the diisonitrile chalkophore-mediated protection of
181 respiration is accompanied by ATP depletion, we measured ATP levels in WT and chalkophore
182 deficient cells treated with copper deprivation or Q203. Copper deprivation with TTM or
183 treatment with Q203 had minimal effect on wild-type cells (Figure 3E), but inhibited ATP
184 production in the Δ*nrp*Δ*cydAB* strain (Figure 3E). Taken together, these data demonstrate that
185 diisonitrile chalkophores maintain oxidative phosphorylation by the heme-copper respiratory
186 oxidase under copper starvation. Because the electron transport path of the $bcc{:}aa_3$ oxidase
187 contains three copper sites, these findings are consistent with a model in which these copper
188 sites become dysfunctional when copper is limiting, leading to impaired supercomplex
189 biosynthesis or function.
190
191 In eukaryotic copper trafficking disorders in which copper becomes limiting in mitochondria,
192 cytochrome C oxidase becomes unstable, preventing assembly (37). To determine if similar
193 mechanism is operative in mycobacterial cells, we inserted an ALFA epitope tag (38) at the C
194 terminus of CtaD in both WT and Δ*nrp* cells and, after confirming functionality (Figure 2E),
195 examined CtaD protein levels with copper deprivation. CtaD levels remained unchanged with
196 either TTM or BCS (Figure 3F, S3B), indicating that copper deprivation is not affecting oxidase
197 biogenesis and is more likely acting on preexisting respiratory oxidase complexes.
198
199 **Chalkophores defend oxidative phosphorylation from nutritional immunity**
200
201 Respiration has emerged as an attractive target for antimycobacterials, with the ATP synthase
202 inhibitor bedaquiline now a cornerstone of MDR TB treatment (39, 40) and Q203 in clinical trials
203 (41). Although it is also clear that ATP generation via oxidative phosphorylation is required for
204 *M. tuberculosis* growth in mice (22, 29, 42, 43), it is less clear whether the reactive centers of
205 the electron transport chain are compromised by the host and whether *M. tuberculosis* must
206 defend or restore the integrity of the electron transport chain during infection. To examine this
207 question, we infected C57BL/6 mice with *M. tuberculosis* strains lacking diisonitrile chalkophore
208 biosynthesis, alone and in combination with deletion of the genes encoding CytBD (Δ*nrp* and
209 Δ*nrp*Δ*cydAB*). The mouse attenuation phenotype of *M. tuberculosis* lacking *nrp* has been
210 reported by several groups (12, 20, 44) and indicates a mild early attenuation phenotype in the
211 lungs. Loss of *cydAB* in the Δ*nrp* background dramatically exacerbated the mild attenuation of

212 diisonitrile chalkophore deficient strain in the lung (Figure 4A) and caused severe attenuation in
213 the spleen (Figure 4B). Complementation with the *nrp* gene restored virulence to wild-type
214 levels, demonstrating that chalkophore mediated protection of the respiratory chain is a critical
215 virulence function of *M. tuberculosis*.
216
217 To investigate the host pressure that targets the respiratory chain, we hypothesized that
218 neutrophils, which express several metal binding proteins such as calprotectin, might be
219 relevant. However, efficient depletion of neutrophils by administration of a Ly6G antibody
220 (Figure S4A, B) did not reverse the severe attenuation of the Δ*nrp*Δ*cydAB* strain in the lungs or
221 spleen (Figure 4C, D). Similarly, infection of SCID mice, which lack adaptive immunity, also had
222 no effect on diisonitrile chalkophore deficient *M. tuberculosis* titers (Figure 4E, F).
223

Discussion

We have identified diisonitrile chalkophore biosynthesis as an *M. tuberculosis* virulence mechanism that defends against copper starvation during infection. Although it is well established that phagosomal pathogens experience both metal excess and metal deprivation in the host, the general paradigm of copper and zinc nutritional immunity is that high phagosomal levels of these metals are deployed as antimicrobial effectors to limit pathogen growth (10, 11, 45-47). Our data indicate that *M. tuberculosis* must also cope with copper deprivation as a host inflicted stress during infection and that *M. tuberculosis* deploys diisonitrile chalkophores to acquire copper in the host. Diisonitrile chalkophores display an extremely high affinity for copper ions (18, 35, 48), and their ability to overcome copper deprivation by strong copper chelators in vitro and host immunity in vivo indicates that they perform an analogous function to bacterial siderophores, which scavenge iron from host iron limitation. Given the abundant data indicating a high copper environment in the macrophage phagosome, the sites and circumstances of the copper deprived niche of *M. tuberculosis* remain to be determined but could include distinct subcellular compartments (i.e. phagosomal vs cytosolic), phases of infection, or bacterial localization within different lung compartments such as cavities.

Although deprivation of metals from pathogens, including iron and zinc, is a well-recognized mechanism of innate immunity, in most cases the specific bacterial targets that ultimately mediate the antimicrobial function of metal deprivation are not clearly defined and are assumed to be pleiotropic due to the numerous essential metal dependent enzymes in the bacterial cell. However, our data indicates that the copper deprivation against which the diisonitrile chalkophore system defends targets a single membrane enzyme complex, the *bcc:aa*$_3$ supercomplex, a heme-copper respiratory oxidase. *M. tuberculosis* deploys two respiratory oxidases, *bcc:aa*$_3$ and CytBD, which are redundant for bacterial viability. This dual oxidase arrangement provides respiratory chain flexibility during chemical inhibition of each oxidase, and some evidence suggests that respiratory chain flexibility promotes host adaptation (22, 42, 43). The copper centers of respiratory oxidases that participate in electron flow to oxygen are conserved from bacteria to mitochondria and represent a membrane exposed electroreactive center susceptible to damage. Our data reveals that *M. tuberculosis* deploys multilayered strategies to maintain oxidative phosphorylation in the face of host immune pressure. In addition, *M. tuberculosis* deploys a backup oxidase, CytBD, which can support *M. tuberculosis* virulence when the *bcc:aa*$_3$ oxidase is dysfunctional, such as when QcrB is inhibited by Q203.

259 However, the role of this backup oxidase in pathogenesis was uncelar. Although CytBD is
260 induced in mouse lung, peaking at 21 days post infection (49), is required for optimal fitness of
261 *M. tuberculosis* in the lung in competition experiments (43), *M. tuberculosis* lacking CytBD is
262 fully virulent (22). Our results reveal the essential role of this compensatory oxidase in
263 virulence, which is only evident when the *bcc:aa*$_3$ oxidase in inactivated in vivo in *M.*
264 *tuberculosis* lacking chalkophore biosynthesis, thereby revealing a complex system for
265 maintaining respiration. These studies further strengthen the rationale for targeting CytBD for
266 antibiotic development (34, 50).
267
268 The respiratory chain of *M. tuberculosis* has emerged as a promising drug target. Our data
269 indicates that diisonitrile chalkophore biosynthesis, as a mechanism of protection for the
270 respiratory chain during infection, may provide an alternative approach to target this critical
271 energy generating system. Beyond its importance as a drug target, this study identifies a new
272 mechanism of resistance to copper deprivation that, in concert with CytBD, is part of a central
273 virulence strategy of *M. tuberculosis* to protect oxidative phosphorylation during infection.
274

Materials and Methods

Reagents

Middlebrook 7H10 Agar, 7H9 Broth, dextrose, Tween-80, bovine serum albumin (BSA), and UltraPure DNase/RNase -free distilled water were purchased from Fisher Scientific. Ammonium tetrathiomolybdate (TTM), bathocuproinedisulfonic acid, disodium salt (BCS), dimethyl sulfoxide (DMSO), copper sulfate, zinc sulfate, magnesium sulfate, calcium chloride, and ATP were purchased from Millipore Sigma. Biotechnology (BT) grade Chelex 100 resin, sodium form, was purchased from BioRad. Q203 (Telacebec) was purchased from AbMole. ND-011992 was synthesized as previously described (29). The diisonitrile lipopeptide analogue was synthesized and characterized as described below.

General growth conditions, strains, and DNA manipulations

M. tuberculosis Erdman WT and mutant stains were grown and maintained in 7H9 media (broth), or on 7H10 (agar) supplemented with 10% OADC (oleic acid, albumin, dextrose, saline), 0.05% glycerol (7H9-OADC/7H10-OADC). Broth cultures were additionally supplemented with 0.02% Tween-80. Chromosomal deletion mutations were generated by specialized transduction utilizing the temperature sensitive phage phAE87. Mutant strains were confirmed by PCR followed by sequencing. For complete strain list with relevant features see **Table S1**. Plasmids utilized in this study were generated using standard molecular techniques and are listed with their features in **Table S2**.

Growth assays

For liquid growth assays, the indicated strains were pre grown in non-chelated media until reaching an OD_{600} value of ~1.0. Cells were then collected by centrifugation (3,700 x *g*, 10 min) and washed twice with chelexed phosphate buffered saline with 0.02% Tween-80 (PBS Tween-80). Growth assays were initiated at a calculated OD_{600} of 0.005 by the addition of 1 mL of washed culture at an OD_{600} of 0.05 to 9 mL of replete 7H9-ADS (albumin, dextrose, saline) generated as described previously (21). TTM, BCS, Q203, ND-011992, and/or synthetic diisonitrile chalkophore were then added at the indicated concentration. Growth at 37°C was assayed via daily OD_{600} measurements.

310

311 For agar growth assays, cells were pre-grown and washed as indicated above. Washed cells
312 were then normalized to an OD_{600} of 0.1, serially diluted from 10^0-10^{-6} in PBS Tween-80, and
313 spotted on to 7H10-OADC plates containing the indicated concentrations of TTM, BCS, or
314 DMSO vehicle control in triplicate. Plates incubated at 37°C, 5% CO_2 were imaged after 14
315 days of incubation to show relative growth, and CFU counts were enumerated after 21 days of
316 incubation.

317

318 **RNA preparation**

319

320 Triplicate 25 mL cultures of strains indicated above were grown in 7H9-ADS until they reached
321 an OD_{600} of 0.3 to 0.5. Cultures were then treated with the indicated concentration of TTM, 100
322 nM Q203, or a DMSO vehicle control, for 5 hrs. Following a duplicate wash with Chelex treated
323 PBS Tween-80, cells were collected by centrifugation (3,700 × *g*, 10 min), suspended, and
324 resuspended in 1 mL of TRIzol reagent. Cells in 1 mL of TRIzol were mechanically disrupted
325 with zirconia beads via 2x45 sec pulses in a BioSpec Mini24 BeadBeater with 5 min intervening
326 rest periods on ice. Following lysis, beads were removed by centrifugation (20,000 × *g,* 5 min)
327 and total RNA was isolated using the Direct-zol RNA miniprep kit (Zymo Research) as directed
328 by the manufacturer.

329

330 **RT-qPCR**

331

332 DNAse treatment of RNA purified as noted above was performed using the Turbo DNA-free kit
333 (Invitrogen). A total of 500 ng of resulting total RNA was used to synthesize cDNA via random
334 priming utilizing the iScript™ cDNA Synthesis Kit (Biorad). Real-time qPCR was performed on
335 QuantStudio 6 Pro (Applied Biosystems) using iTaq Universal SYBR Green Supermix (Biorad).
336 For *cydA* expression, normalized cycle threshold (CT) was determined relative to the
337 housekeeping gene *sigA*. Reactions with reverse transcriptase were included for each sample
338 and excluded DNA contamination as a source of amplification signal. Relative expression level
339 was calculated using the formula 2−(CT*cydA*-CT*sigA*). Sequences of gene specific primers are
340 as follows: For *cydA,* 5'-GTCATCGAAGTGCCCTATGT-3' and 5'-
341 CTGGTATTCCTGCTGCAGAT-3', and for *sigA,* 5'- CGTCTTCATCCCAGACGAAAT-3' and 5'-
342 CGACGAAGACCACGAAGAC-3'.

343

344 **RNA Sequencing and Data Analysis**

345

346 After RiboGreen quantification and quality control by Agilent BioAnalyzer, 500 ng of total RNA
347 underwent ribosomal depletion with the NEBNext rRNA Depletion Kit (Bacteria) (NEB catalog #
348 E7850) and library preparation with the TruSeq Stranded Total RNA LT Kit (Illumina catalog #
349 RS-122-1202) according to instructions provided by the manufacturer with 8 cycles of PCR.
350 Samples were barcoded and run on a NovaSeq 6000 in a PE100 run, using the NovaSeq 6000
351 S4 Reagent Kit (200 Cycles) (Illumina). On average, 27 million paired reads were generated
352 per sample. Post-run demultiplexing and adapter removal were performed and fastq files were
353 inspected using fastqc (51). Trimmed fastq files were then aligned to the reference genome (*M.*
354 *tuberculosis* H37Rv; NC_000962.3) using bwa mem (52). Bam files were sorted and merged
355 using samtools (53) and gene counts were obtained using featureCounts from the Bioconductor
356 Rsubread package (54). Differentially expressed genes were identified using the DESeq2 R
357 package (55) and subsequent analysis of gene expression was performed in (56, 57).

358

359 **Immunoblotting**

360

361 Duplicate 20 mL cultures of chelated 7H9-ADS replete for all ions were inoculated at an OD_{600}
362 of 0.02. Upon reaching an OD_{600} of 0.6-0.7, cultures were treated with the indicated
363 concentration of TTM, or DMSO vehicle control, for 24 hrs. Cells were collected by
364 centrifugation (3700 x *g*, 10 min) washed once with 1mL of lysis buffer (350 mM sodium
365 chloride, 20 mM Tris pH 8.0, 1 mM 2-mercaptoethanol) prior to suspension in 0.8 mL of lysis
366 buffer plus ~100µL of zirconia beads. Lysis was performed by 3x45 sec pulses in a BioSpec
367 Mini24 beadbeater with 5 min intervening rest periods on ice. Beads and debris were removed
368 by centrifugation at 20,000 x *g* for 15 min at 4°C, the resulting supernatant was mixed 1:1 with
369 2x Laemmli sample buffer supplemented with 0.1 M dithiothreitol (DTT). 20 µL of each sample,
370 heated for 10 min at 100ºC, was then separated on 4-12% NuPAGE Bis-Tris poly acrylamide
371 gels. Separated proteins were transferred to nitrocellulose and probed with the indicated
372 antibodies. Antibodies used in this study are: monoclonal anti-*E. coli* RNA -polymerase β
373 (BioLegend), sdAb anti-ALFA tag-HRP (NanoTag Biotechnologies). Chemiluminescence was
374 visualized using SuperSignal™West Pico Plus chemiluminescent substrate (Thermo Scientific).
375 Blots were imaged on an iBright FL1000 imager (Themo Fisher Scientific). CtaD ALFA blots
376 were quantitated using ImageJ software. Relative ALFA signal was normalized to corresponding
377 Rpoβ loading control levels.

378

379 **Methylene blue assay**

380 Cultures were grown in 7H9-ADS until they reached an OD_{600} of 0.5-0.7 which were then
381 washed twice in chelexed PBS Tween-80. OD_{600} of cultures were adjusted to 0.15 with fresh
382 7H9-ADS and incubated with indicated concentrations of TTM, Q203, ND-011992, or DMSO
383 vehicle control, for 4 hrs. Following incubation, 4-ml screw-cap glass vials were filled with the
384 cultures and methylene blue dye was added at a final concentration of 0.001%. All vials were
385 sealed tightly using a PTFE/rubber seal (Thermo Scientific) and incubated at 37°C in an
386 anaerobic container (Benton Dickinson GasPak EZ container systems) for 3 days.

387

388 **Oxygen Consumption Measurements**

389 Oxygen consumption was assessed using PSt6 sensor spots and a Fibox 4 trace instrument
390 (PreSens Precision Sensing GmbH Am BioPark, Germany)(36). Screw cap glass vials (Thermo
391 Scientific) containing the sensor spot PSt6 were filled with cultures grown in 7H9-ADS at a
392 calculated OD_{600} of 0.005 and the indicated concentrations of TTM, Q203, ND-011992, or
393 DMSO vehicle control. The vials were tightly sealed using a PTFE/rubber seal (Thermo
394 Scientific) and incubated at 37°C in an anaerobic pouch (Benton Dickinson GasPak EZ pouch
395 systems). Percent oxygen was measured daily via the Fibox 4 trace oxygen meter without
396 unsealing the anaerobic environment.

397

398 **ATP quantitation**

399 ATP levels were quantified with the BacTiter-Glo™ reagent (Promega). The indicated strains
400 were first pre-grown to an OD_{600} of 0.5-1.0 in 7H9-OADC. Cells were then washed twice with
401 PBS Tween-80 and suspended in 7H9-OADC at an OD_{600} of 0.05. 96-Well plates were
402 inoculated with 100 μL of washed culture in replicate wells. The indicated concentrations of
403 TTM, Q203, or DMSO vehicle control were then added, and plates were incubated at 37°C,
404 0.05% CO_2 for 24 hrs. 100 μL of BacTiter-Glo was then added to each well and plates were
405 incubated 15 additional mins at 37°C, 5% CO_2 prior to reading on a SpectraMax M3 plate
406 reader. [ATP] in test samples was quantified against standard curves of ATP.

407

408 **Synthesis of diisonitrile chalkophores**

409

410 Details of synthesis and characterization are provided in SI Appendix 1.

411

412 **Aerosol infection of mice**

413

414 8–10-week-old C57BL/6J (stock number 00064) and 8-10 week B6.Cg-*Prkdc*^{scid}/*SzJ* (stock
415 number 001913, RRID: IMSR_JAX:001913) were purchased from The Jackson Laboratory. All
416 purchased mice were rested within our animal facility to normalize microbiota for 2 weeks. Care,
417 housing, and experimentation on laboratory mice were performed in accordance with the
418 National Institute of Heath guidelines, and the approval of the Memorial Sloan Kettering
419 Institutional Animal Care and Use Committee (IACUC). Strains for infection were grown to an
420 OD_{600} of 0.5-0.7 in 7H9-OADC, washed twice with PBS Tween-80 followed by brief sonication to
421 disrupt aggregates. Final inoculums were prepared by suspending $8x10^7$ CFU in 10 mL of sterile
422 water. Mice were exposed to $4x10^7$ CFU in a Glas-Col aerosol exposure unit, a dose calibrated
423 to deliver 10-50 CFU per mouse. At the indicated time points post infection, 5 individual mice
424 were humanely euthanized and both lungs and spleens were harvested for CFU determination.
425 Organ homogenates were cultured on 7H10-OADC plates, and CFU was enumerated after 28
426 days of incubation at 37ºC, 5% CO_2. 20 additional SCID mice (10: WT *M. tuberculosis*, 10:
427 Δ*nrp*Δ*cydAB*) infected as described above, were used to assess survival. Infected mice were
428 monitored daily and humanely euthanized upon frank signs of morbidity.
429
430 **Neutrophil depletion**
431
432 Mice were treated intraperitoneally with anti-Ly6G (BioXcell, clone 1A8, RRID AB_1107721) or
433 isotype control (BioXcell, clone 2A3, RRID AB_1107769) every 48 hrs. Lungs were harvested
434 aseptically and single cell suspensions prepared by homogenization in a Bullet Blender with 2.0
435 mM zirconium oxide beads for 3 min followed by 100 micron filtration. After lysis of red blood
436 cells with Gibco ACK lysing buffer and blocking of Fc receptors (Invitrogen CD16/CD32 clone
437 93, RRID AB_467133), cells were stained with live/dead aqua (Thermo) and antibodies to
438 CD45 (FITC, clone 30-F11, BD Biosciences, RRID AB_394609), CD11b (BUV661, clone M1/70,
439 BD Biosciences), CD11c (APC-R700, clone N418, RRID AB_2744277), Ly6C (BV605, clone
440 AL-21, BD Biosciences, AB_2737949), CD80 (PerCP Cy5.5, clone 16-10A1 AB_1727514),
441 CD86 (Pacific Blue, clone GL-1, BioLegend, RRID AB_493466), MHC II (BUV395, clone 2G9,
442 BD Biosciences RRID AB_2741827), GR1 (PE, clone RB6-8C5, BD Biosciences, RRID
443 AB_398532), and Ly6G (APC, clone 1A8, BD Biosciences, RRID AB_394208) and analyzed by
444 flow cytometry on a BD Fortessa cytometer after paraformaldehyde fixation.
445
446
447
448
449

Acknowledgements

This work was supported by R01AI138446 and P30 CA008748. We acknowledge the use of the Integrated Genomics Operation Core, funded by the NCI Cancer Center Support Grant (CCSG, P30 CA08748), Cycle for Survival, and the Marie-Josée and Henry R. Kravis Center for Molecular Oncology. We thank Christina Stallings for advice about neutrophil depletion, James Bean for RNAseq analysis, and George Sukenick and Rui Wang (MSK) for expert NMR and mass spectral support.

Author Contributions

J.A.B., Y.O., and M.S.G. conceived and planned the experiments. C.H. synthesized the diisonitrile analogue under the supervision of D.T. J.A.B., Y.O., and M.S.G. carried out the experiments with support and technical expertise from A.B. for neutrophil depletion. J.A.B., Y.O., C.H., D.T., and M.S.G. contributed to the interpretation of the results. M.S.G. took the lead in writing the manuscript. All authors provided critical feedback and helped shape the research, analysis, and manuscript.

Conflicts of Interest

MSG declares equity and consulting fees from Vedanta biosciences and consulting fees from Fimbrion therapeutics. DST declares no conflicts of interest pertaining to this work.

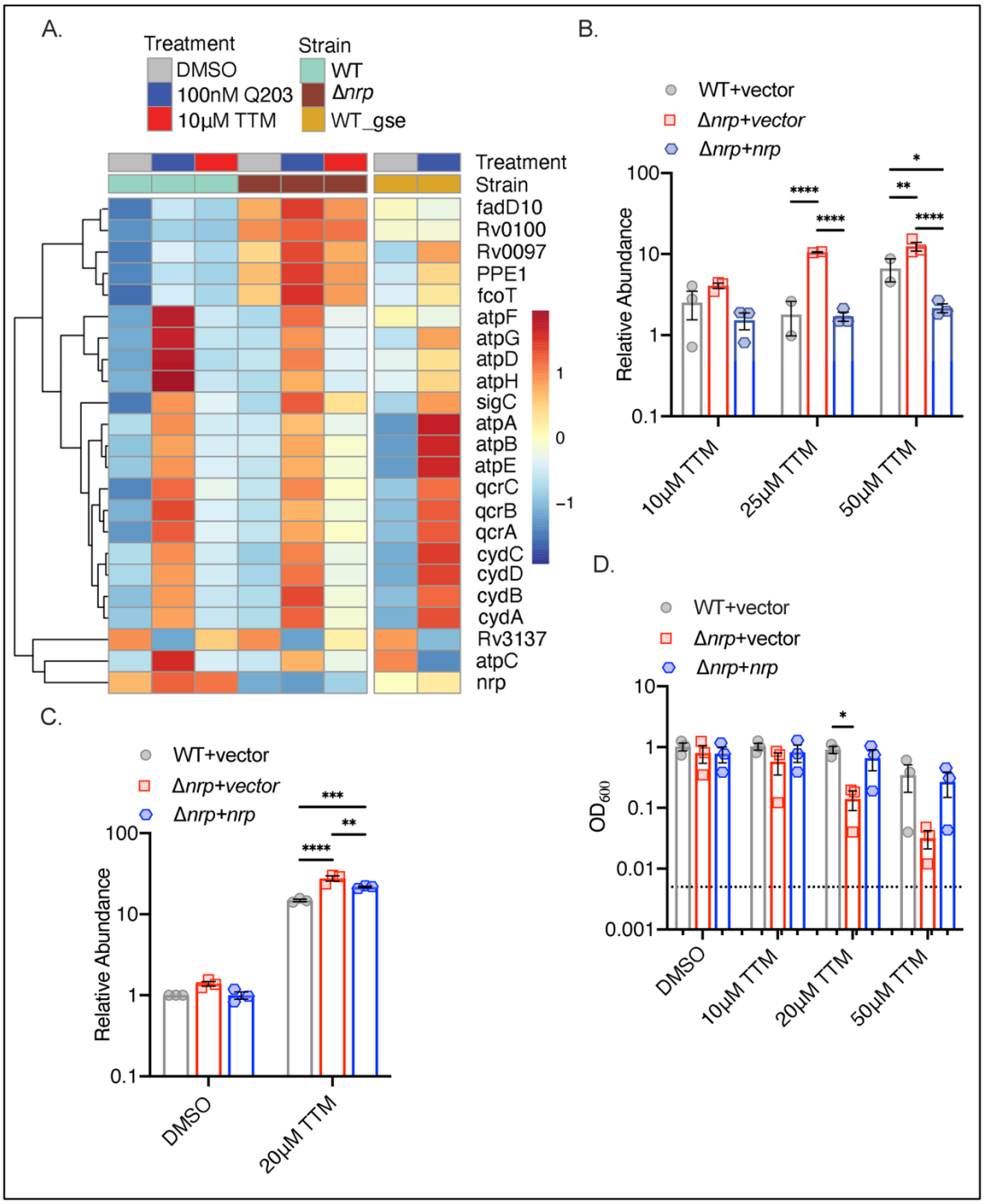

Figure 1 Copper deprivation in chalkophore-deficient *M. tuberculosis* mimics *bcc:aa*$_3$ oxidase inhibition

A. Heat map of transcripts encoding selected respiratory chain components determined by RNA sequencing of *M. tuberculosis* WT or Δ*nrp* treated with TTM or Q203. WT_GSE is the published dataset GSE159080 of *M. tuberculosis* H37Rv treated with Q203.

486 **B.** RT-qPCR of the transcript encoding CydA in *M. tuberculosis* WT, Δ*nrp*, and
487 complemented strain treated with varying TTM concentrations for 4 hours. Error bars
488 represent standard error of the mean (SEM). Statistical significance determined via two-
489 way ANOVA with Tukey correction for multiple comparisons. *=p<0.05, **=p<0.01, ****=
490 p<0.0001.
491 **C.** RT-qPCR of the transcript encoding CydA in *M. tuberculosis* WT, Δ*nrp*, and
492 complemented strain treated with 20 μM TTM for 24 hours. Error bars are SEM.
493 Statistical significance determined via two-way ANOVA with Tukey correction for multiple
494 comparisons. **=p<0.01, ***=p<0.001, ****= p<0.0001.
495 **D.** Dose dependent effect of TTM on growth of the indicated *M. tuberculosis* strains at 7
496 days post inoculation. The dotted line indicates the starting inoculum. Error bars are
497 SEM. Statistical significance determined via two-way ANOVA with Tukey correction for
498 multiple comparisons. *=p<0.05.

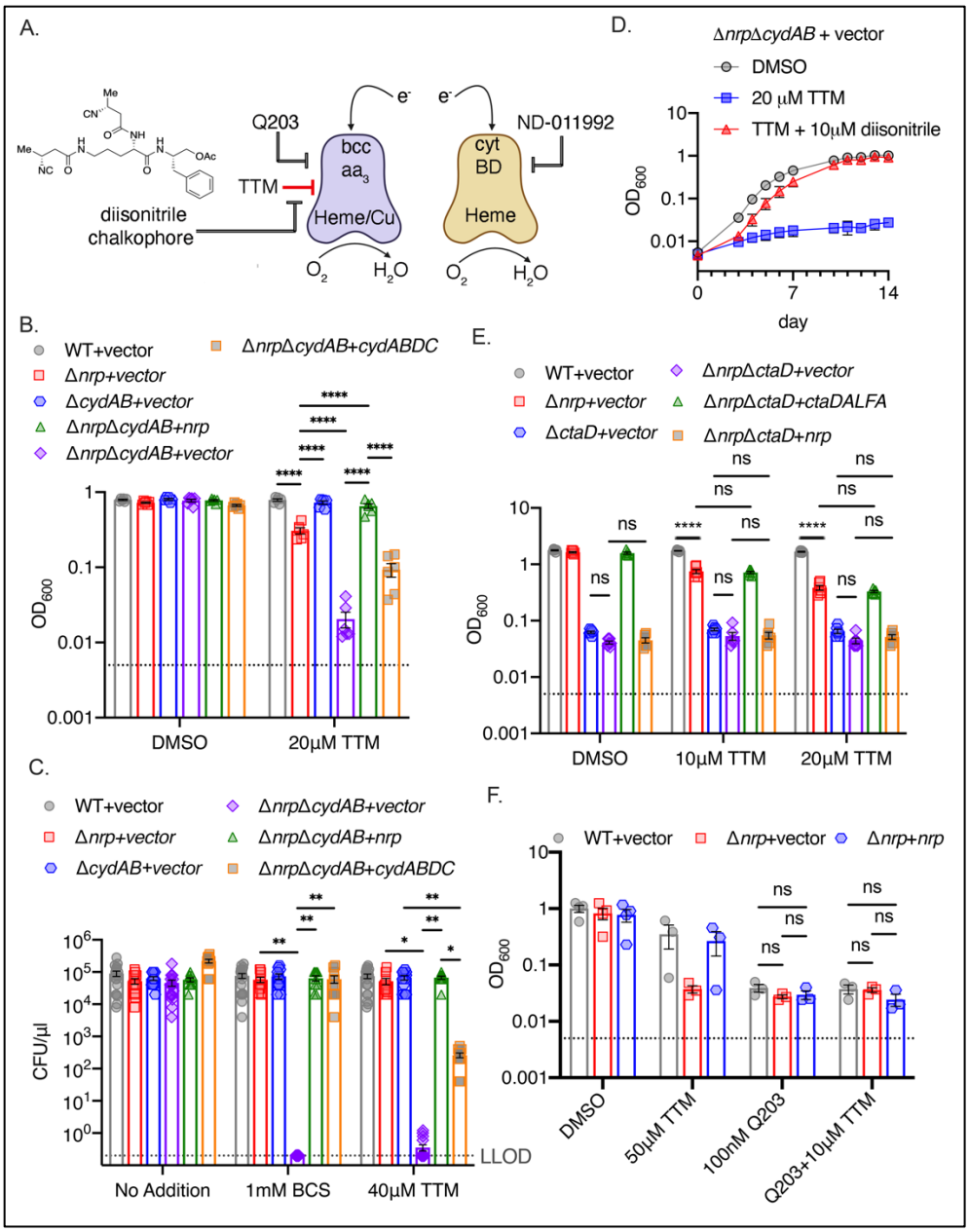

Figure 2 Chalkophores maintain *M. tuberculosis* viability through the heme-copper *bcc:aa$_3$* oxidase during copper starvation

A. Schematic of the terminal respiratory oxidases of *M. tuberculosis*. The *bcc:aa$_3$* oxidase is a heme-copper oxidase and CytBD is a copper-independent heme oxidase. Both transfer electrons to oxygen. Q203 is an inhibitor of *bcc:aa$_3$* by targeting the QcrB subunit, whereas ND-011992 targets CytBD. The two oxidases are individually dispensable due to compensation by the other oxidase, but *M. tuberculosis* lacking both is nonviable. The model to be tested is that copper chelation deprives the *bcc:aa$_3$*

508 oxidase of copper and that diisonitrile chalkophores counter this copper deprivation
509 stress.
510 B. Liquid growth assays of the indicated strains with or without 20 μM TTM treatment.
511 OD_{600} at day 10 post inoculation displayed. Dotted line indicates starting inoculum. Error
512 bars are SEM. Statistical significance determined via two-way ANOVA with Tukey
513 correction for multiple comparisons. ****= $p<0.0001$.
514 C. Bacterial survival of the indicated strains on agar media containing DMSO, 1 mM
515 BCS or 40 μM TTM. Dotted line indicates lower limit of detection (LLOD). Error bars are
516 SEM. Statistical significance determined via two-way ANOVA with Tukey correction for
517 multiple comparisons. **= $p<0.01$, *=$p<0.05$
518 D. The copper deprivation sensitivity of *M. tuberculosis* Δ*nrp*Δ*cydAB* strain can be
519 rescued with a synthetic diisonitrile chalkophore. Liquid growth assays of Δ*nrp*Δ*cydAB*
520 with DMSO, 20 μM TTM, or 20 μM TTM with 10 μM of the diisonitrile chalkophore
521 pictured in panel A. Error bars are SEM.
522 E. The *bcc:aa*$_3$ oxidase is the only target of copper starvation countered by diisonitrile
523 chalkophores. Liquid growth assays of the indicated strains treated with 10 or 20 μM
524 TTM, or DMSO vehicle control. OD_{600} at day 10 post inoculation displayed. Dotted line
525 indicates starting inoculum. Error bars are SEM. Statistical significance determined via
526 two-way ANOVA with Tukey correction for multiple comparisons. ns= not significant,
527 ****= $p<0.0001$.
528 F. The effect of copper deprivation is masked by inhibition of QcrB subunit of *bcc*:*aa*$_3$.
529 Liquid growth assays of the indicated strains treated with TTM or Q203 alone or co-
530 treated with both at the indicated concentrations. OD_{600} at day 7 post inoculation
531 displayed. Dotted line indicates starting inoculum. Error bars are SEM. Statistical
532 significance determined via two-way ANOVA with Tukey correction for multiple
533 comparisons. ns= not significant.
534

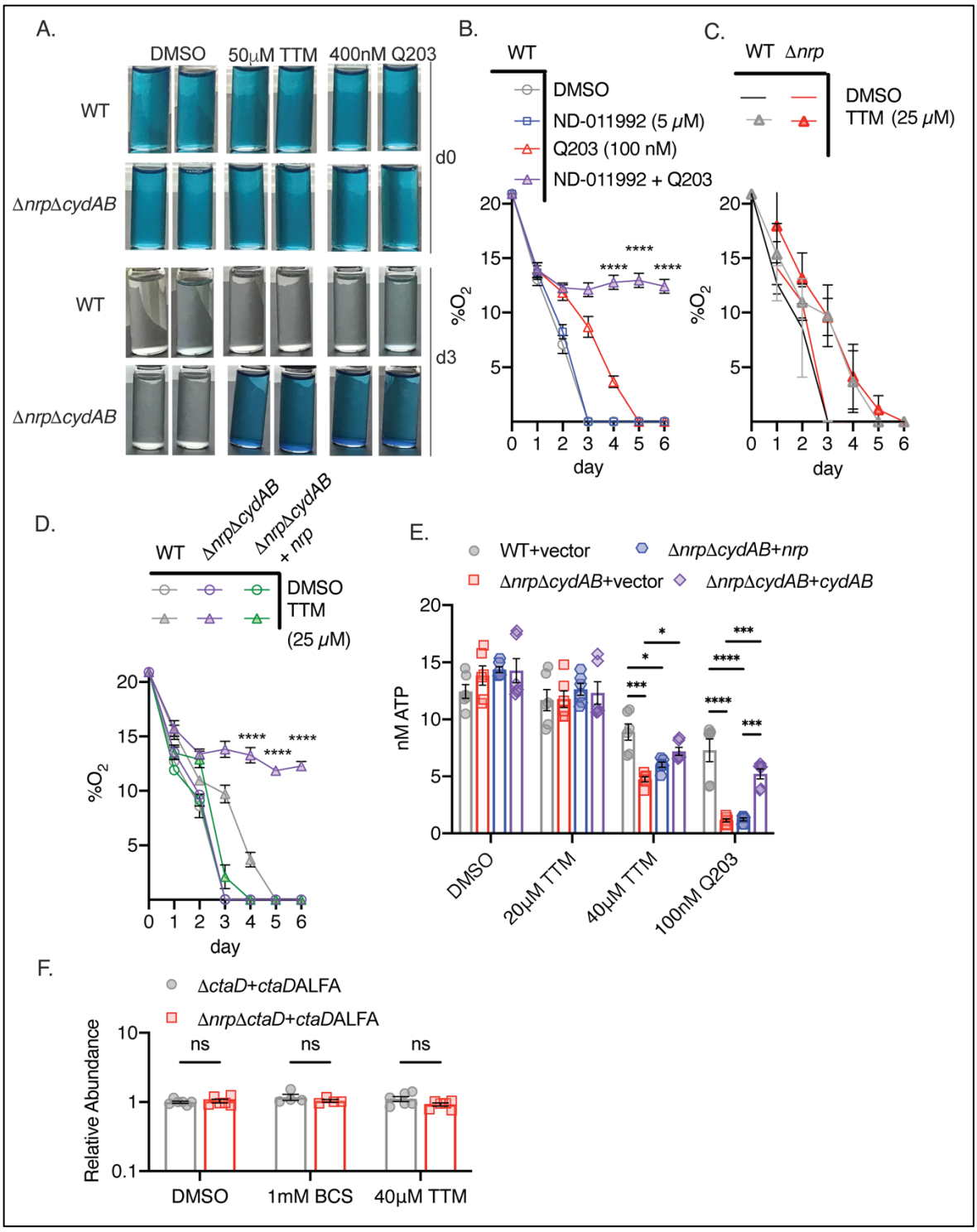

Figure 3 Chalkophore biosynthesis maintains oxidative phosphorylation through the heme-copper *bcc:aa₃* oxidase

538 **A.** Methylene blue decolorization assay of oxygen consumption under copper deprivation
539 (TTM) or treatment with Q203 in WT or Δ*nrp*Δ*cydAB M. tuberculosis*. Clear vials indicate
540 oxygen consumption by respiration.
541 **B.** Quantitative measurement of oxygen consumption using oxygen sensitive optical
542 sensors. WT *M. tuberculosis* treated with DMSO, ND-011992, Q203, or both ND-011992
543 and Q203. Oxygen measurements were taken daily. Each point represents three
544 measurements of two biologic replicates. Error bars are SEM. Statistical significance
545 between Q203 and ND-011992 + Q203 determined via two-way ANOVA with Tukey
546 correction for multiple comparisons. ****= $p<0.0001$.
547 **C.** Same assay as in panel B with WT and Δ*nrp M. tuberculosis* treated with DMSO or 25
548 μM TTM. Error bars are SEM.
549 **D.** Same assay as in panel B with WT, Δ*nrp*Δ*cydAB,* or Δ*nrp*Δ*cydAB* + *nrp* treated with 25
550 μM TTM. Error bars are SEM. Statistical significance between WT and Δ*nrp*Δ*cydAB*
551 treated with 25 μM TTM determined via two-way ANOVA with Tukey correction for
552 multiple comparisons. ****= $p<0.0001$.
553 **E.** Cellular ATP levels determined by BacTiter-Glo in the indicated strains treated with
554 DMSO, 20 or 40 μM TTM, or 100 nM Q203. [ATP] determined by standard curve
555 determined in growth media containing the same quantities of DMSO, TTM or Q203.
556 Error bars are SEM. Statistical significance determined via two-way ANOVA with Tukey
557 correction for multiple comparisons. *= $p<0.05$, ***=$p<0.001$, ****=$p<0.0001$.
558 **F.** Relative abundance of a CtaD-ALFA protein in *M. tuberculosis* of the indicated genotype
559 treated with BCS or TTM. See Figure S3 for primary immunoblot data. Error bars are
560 SEM. Statistical significance determined via two-way ANOVA with Tukey correction for
561 multiple comparisons. ns= not significant.
562

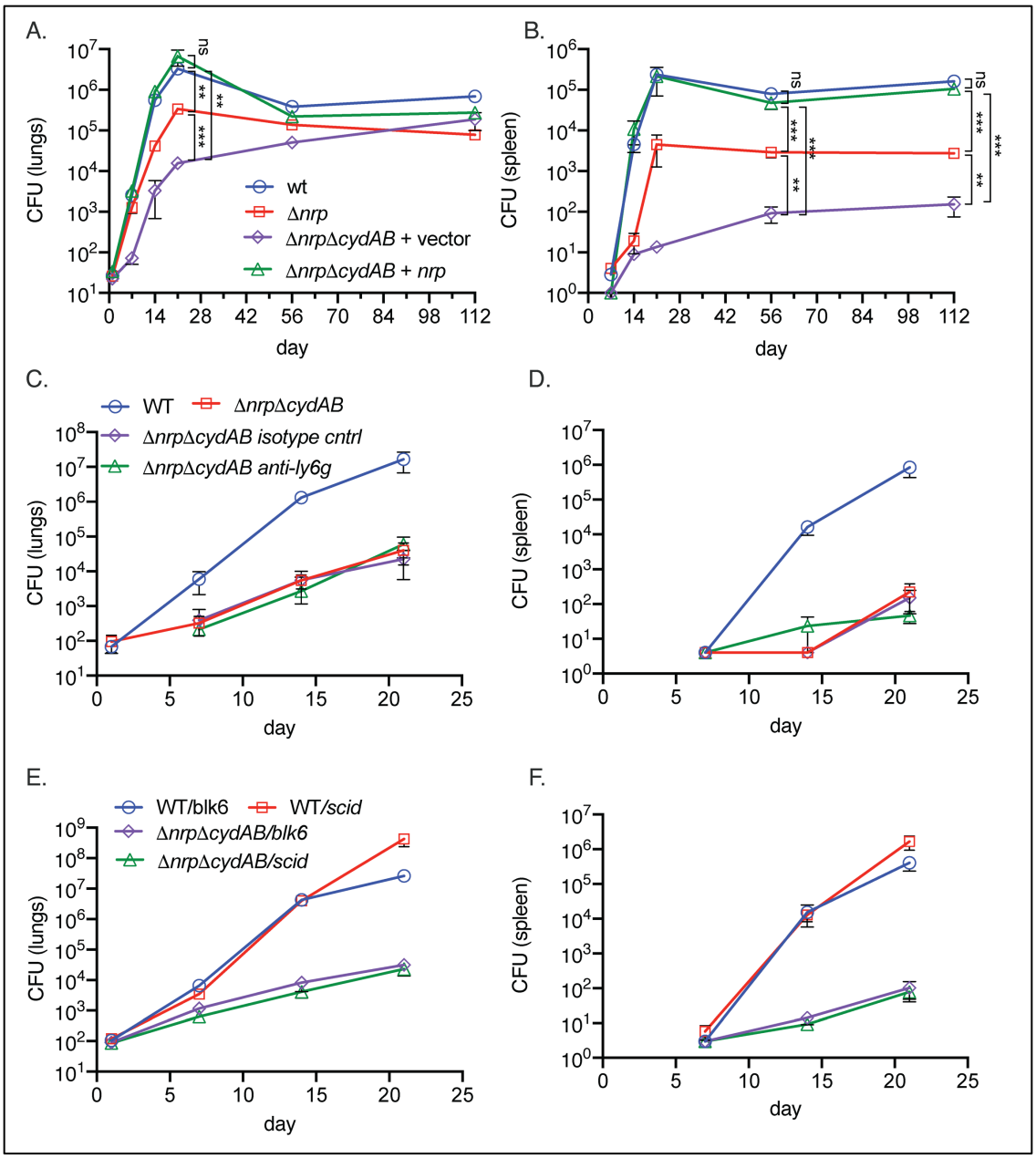

Figure 4 Respiratory chain flexibility is critical for *M. tuberculosis* virulence

A, B. Bacterial titers in the lung (A) or spleen (B) in mice infected with *M. tuberculosis* WT, Δ*nrp*, Δ*nrp*Δ*cydAB,* or Δ*nrp*Δ*cydAB* + *nrp.* Error bars are SEM. Statistical significance determined via two-way ANOVA with Tukey correction for multiple comparisons. Not significant (ns), **=p<0.01, and ***=p<0.001.

C, D. Copper deprivation by the host is independent of neutrophils. Bacterial titers in the lung (C) or spleen (D) in mice infected with *M. tuberculosis* WT or Δ*nrp*Δ*cydAB,* or

573 Δ*nrp*Δ*cydAB* + *nrp* treated with isotype control antibodies or anti-Ly6G antibodies to deplete
574 neutrophils. Error bars are SEM.
575
576 E, F. Copper deprivation by the host is independent of adaptive immunity. Bacterial
577 titers in the lung (E) or spleen (F) in C57BL/6J or C57BL/6 SCID mice infected with *M.*
578 *tuberculosis* WT or Δ*nrp*Δ*cydAB.* Error bars are SEM.
579
580
581
582
583

584 **References**

585

586 1. Murdoch CC, Skaar EP. 2022. Nutritional immunity: the battle for nutrient metals at the
587 host–pathogen interface. Nature Reviews Microbiology doi:10.1038/s41579-022-00745-
588 6.
589 2. Sheldon JR, Laakso HA, Heinrichs DE. 2016. Iron Acquisition Strategies of Bacterial
590 Pathogens. Microbiology Spectrum 4:10.1128/microbiolspec.vmbf-0010-2015.
591 3. Behnsen J, Zhi H, Aron AT, Subramanian V, Santus W, Lee MH, Gerner RR, Petras D,
592 Liu JZ, Green KD, Price SL, Camacho J, Hillman H, Tjokrosurjo J, Montaldo NP, Hoover
593 EM, Treacy-Abarca S, Gilston BA, Skaar EP, Chazin WJ, Garneau-Tsodikova S,
594 Lawrenz MB, Perry RD, Nuccio SP, Dorrestein PC, Raffatellu M. 2021. Siderophore-
595 mediated zinc acquisition enhances enterobacterial colonization of the inflamed gut. Nat
596 Commun 12:7016.
597 4. Bobrov AG, Kirillina O, Fetherston JD, Miller MC, Burlison JA, Perry RD. 2014. The Y
598 ersinia pestis siderophore, yersiniabactin, and the ZnuABC system both contribute to
599 zinc acquisition and the development of lethal septicaemic plague in mice. Molecular
600 microbiology 93:759-775.
601 5. Diaz-Ochoa VE, Lam D, Lee CS, Klaus S, Behnsen J, Liu JZ, Chim N, Nuccio SP, Rathi
602 SG, Mastroianni JR, Edwards RA, Jacobo CM, Cerasi M, Battistoni A, Ouellette AJ,
603 Goulding CW, Chazin WJ, Skaar EP, Raffatellu M. 2016. Salmonella Mitigates Oxidative
604 Stress and Thrives in the Inflamed Gut by Evading Calprotectin-Mediated Manganese
605 Sequestration. Cell Host Microbe 19:814-25.
606 6. Liu JZ, Jellbauer S, Poe AJ, Ton V, Pesciaroli M, Kehl-Fie TE, Restrepo NA, Hosking
607 MP, Edwards RA, Battistoni A, Pasquali P, Lane TE, Chazin WJ, Vogl T, Roth J, Skaar
608 EP, Raffatellu M. 2012. Zinc sequestration by the neutrophil protein calprotectin
609 enhances Salmonella growth in the inflamed gut. Cell Host Microbe 11:227-39.
610 7. Nairn BL, Lonergan ZR, Wang J, Braymer JJ, Zhang Y, Calcutt MW, Lisher JP, Gilston
611 BA, Chazin WJ, de Crécy-Lagard V, Giedroc DP, Skaar EP. 2016. The Response of
612 Acinetobacter baumannii to Zinc Starvation. Cell Host Microbe 19:826-36.
613 8. Sheldon JR, Skaar EP. 2019. Metals as phagocyte antimicrobial effectors. Curr Opin
614 Immunol 60:1-9.
615 9. Shi X, Darwin KH. 2015. Copper homeostasis in Mycobacterium tuberculosis.
616 Metallomics 7:929-34.

617 10. Shi X, Festa RA, Ioerger TR, Butler-Wu S, Sacchettini JC, Darwin KH, Samanovic MI.
618 2014. The copper-responsive RicR regulon contributes to Mycobacterium tuberculosis
619 virulence. mBio 5.
620 11. Festa RA, Jones MB, Butler-Wu S, Sinsimer D, Gerads R, Bishai WR, Peterson SN,
621 Darwin KH. 2011. A novel copper-responsive regulon in Mycobacterium tuberculosis.
622 Mol Microbiol 79:133-48.
623 12. Buglino JA, Sankhe GD, Lazar N, Bean JM, Glickman MS. 2021. Integrated sensing of
624 host stresses by inhibition of a cytoplasmic two-component system controls M.
625 tuberculosis acute lung infection. Elife 10.
626 13. Rowland JL, Niederweis M. 2012. Resistance mechanisms of Mycobacterium
627 tuberculosis against phagosomal copper overload. Tuberculosis (Edinb) 92:202-10.
628 14. Wolschendorf F, Ackart D, Shrestha TB, Hascall-Dove L, Nolan S, Lamichhane G, Wang
629 Y, Bossmann SH, Basaraba RJ, Niederweis M. 2011. Copper resistance is essential for
630 virulence of Mycobacterium tuberculosis. Proceedings of the National Academy of
631 Sciences 108:1621-1626.
632 15. Wagner D, Maser J, Lai B, Cai Z, Barry CE, Höner zu Bentrup K, Russell DG, Bermudez
633 LE. 2005. Elemental Analysis of Mycobacterium avium-,
634 Mycobacterium tuberculosis-, and Mycobacterium smegmatis-
635 Containing Phagosomes Indicates Pathogen-Induced Microenvironments within the Host
636 Cell's Endosomal System. The Journal of Immunology 174:1491-1500.
637 16. Dow A, Sule P, O'Donnell TJ, Burger A, Mattila JT, Antonio B, Vergara K, Marcantonio
638 E, Adams LG, James N, Williams PG, Cirillo JD, Prisic S. 2021. Zinc limitation triggers
639 anticipatory adaptations in Mycobacterium tuberculosis. PLoS Pathog 17:e1009570.
640 17. Harris NC, Born DA, Cai W, Huang Y, Martin J, Khalaf R, Drennan CL, Zhang W. 2018.
641 Isonitrile Formation by a Non-Heme Iron(II)-Dependent Oxidase/Decarboxylase.
642 Angewandte Chemie International Edition 57:9707-9710.
643 18. Wang L, Zhu M, Zhang Q, Zhang X, Yang P, Liu Z, Deng Y, Zhu Y, Huang X, Han L, Li
644 S, He J. 2017. Diisonitrile Natural Product SF2768 Functions As a Chalkophore That
645 Mediates Copper Acquisition in Streptomyces thioluteus. ACS Chem Biol 12:3067-3075.
646 19. Harris NC, Sato M, Herman NA, Twigg F, Cai W, Liu J, Zhu X, Downey J, Khalaf R,
647 Martin J, Koshino H, Zhang W. 2017. Biosynthesis of isonitrile lipopeptides by conserved
648 nonribosomal peptide synthetase gene clusters in Actinobacteria. Proc Natl Acad Sci U
649 S A 114:7025-7030.

650 20. Mehdiratta K, Singh S, Sharma S, Bhosale RS, Choudhury R, Masal DP, Manocha A,
651 Dhamale BD, Khan N, Asokachandran V, Sharma P, Ikeh M, Brown AC, Parish T, Ojha
652 AK, Michael JS, Faruq M, Medigeshi GR, Mohanty D, Reddy DS, Natarajan VT, Kamat
653 SS, Gokhale RS. 2022. Kupyaphores are zinc homeostatic metallophores required for
654 colonization of Mycobacterium tuberculosis. Proc Natl Acad Sci U S A 119.
655 21. Buglino JA, Ozakman Y, Xu Y, Chowdhury F, Tan DS, Glickman MS. 2022. Diisonitrile
656 Lipopeptides Mediate Resistance to Copper Starvation in Pathogenic Mycobacteria.
657 mBio 13:e0251322.
658 22. Kalia NP, Hasenoehrl EJ, Ab Rahman NB, Koh VH, Ang MLT, Sajorda DR, Hards K,
659 Grüber G, Alonso S, Cook GM, Berney M, Pethe K. 2017. Exploiting the synthetic
660 lethality between terminal respiratory oxidases to kill Mycobacterium
661 tuberculosis and clear host infection. Proceedings of the National Academy of
662 Sciences 114:7426-7431.
663 23. Matsoso LG, Kana BD, Crellin PK, Lea-Smith DJ, Pelosi A, Powell D, Dawes SS, Rubin
664 H, Coppel RL, Mizrahi V. 2005. Function of the cytochrome bc1-aa3 branch of the
665 respiratory network in mycobacteria and network adaptation occurring in response to its
666 disruption. J Bacteriol 187:6300-8.
667 24. Lamprecht DA, Finin PM, Rahman MA, Cumming BM, Russell SL, Jonnala SR,
668 Adamson JH, Steyn AJ. 2016. Turning the respiratory flexibility of Mycobacterium
669 tuberculosis against itself. Nat Commun 7:12393.
670 25. Harrison GA, Mayer Bridwell AE, Singh M, Jayaraman K, Weiss LA, Kinsella RL, Aneke
671 JS, Flentie K, Schene ME, Gaggioli M, Solomon SD, Wildman SA, Meyers MJ, Stallings
672 CL. 2019. Identification of 4-Amino-Thieno[2,3-d]Pyrimidines as QcrB Inhibitors in
673 Mycobacterium tuberculosis. mSphere 4.
674 26. O'Malley T, Alling T, Early JV, Wescott HA, Kumar A, Moraski GC, Miller MJ, Masquelin
675 T, Hipskind PA, Parish T. 2018. Imidazopyridine Compounds Inhibit Mycobacterial
676 Growth by Depleting ATP Levels. Antimicrob Agents Chemother 62.
677 27. Lupien A, Foo CS, Savina S, Vocat A, Piton J, Monakhova N, Benjak A, Lamprecht DA,
678 Steyn AJC, Pethe K, Makarov VA, Cole ST. 2020. New 2-Ethylthio-4-
679 methylaminoquinazoline derivatives inhibiting two subunits of cytochrome bc1 in
680 Mycobacterium tuberculosis. PLoS Pathog 16:e1008270.
681 28. Foo CS, Lupien A, Kienle M, Vocat A, Benjak A, Sommer R, Lamprecht DA, Steyn AJC,
682 Pethe K, Piton J, Altmann KH, Cole ST. 2018. Arylvinylpiperazine Amides, a New Class
683 of Potent Inhibitors Targeting QcrB of Mycobacterium tuberculosis. mBio 9.

684 29. Lee BS, Hards K, Engelhart CA, Hasenoehrl EJ, Kalia NP, Mackenzie JS, Sviriaeva E,
685 Chong SMS, Manimekalai MSS, Koh VH, Chan J, Xu J, Alonso S, Miller MJ, Steyn AJC,
686 Gruber G, Schnappinger D, Berney M, Cook GM, Moraski GC, Pethe K. 2021. Dual
687 inhibition of the terminal oxidases eradicates antibiotic-tolerant Mycobacterium
688 tuberculosis. EMBO Mol Med 13:e13207.
689 30. Gong H, Li J, Xu A, Tang Y, Ji W, Gao R, Wang S, Yu L, Tian C, Li J, Yen HY, Man Lam
690 S, Shui G, Yang X, Sun Y, Li X, Jia M, Yang C, Jiang B, Lou Z, Robinson CV, Wong LL,
691 Guddat LW, Sun F, Wang Q, Rao Z. 2018. An electron transfer path connects subunits
692 of a mycobacterial respiratory supercomplex. Science 362.
693 31. Kim MS, Jang J, Ab Rahman NB, Pethe K, Berry EA, Huang LS. 2015. Isolation and
694 Characterization of a Hybrid Respiratory Supercomplex Consisting of Mycobacterium
695 tuberculosis Cytochrome bcc and Mycobacterium smegmatis Cytochrome aa3. J Biol
696 Chem 290:14350-60.
697 32. Mathiyazakan V, Wong CF, Harikishore A, Pethe K, Grüber G. 2023. Cryo-Electron
698 Microscopy Structure of the Mycobacterium tuberculosis Cytochrome bcc:aa(3)
699 Supercomplex and a Novel Inhibitor Targeting Subunit Cytochrome cI. Antimicrob
700 Agents Chemother 67:e0153122.
701 33. Wiseman B, Nitharwal RG, Fedotovskaya O, Schäfer J, Guo H, Kuang Q, Benlekbir S,
702 Sjöstrand D, Ädelroth P, Rubinstein JL, Brzezinski P, Högbom M. 2018. Structure of a
703 functional obligate complex III(2)IV(2) respiratory supercomplex from Mycobacterium
704 smegmatis. Nat Struct Mol Biol 25:1128-1136.
705 34. Safarian S, Opel-Reading HK, Wu D, Mehdipour AR, Hards K, Harold LK, Radloff M,
706 Stewart I, Welsch S, Hummer G. 2021. The cryo-EM structure of the bd oxidase from M.
707 tuberculosis reveals a unique structural framework and enables rational drug design to
708 combat TB. Nature Communications 12:5236.
709 35. Xu Y, Tan DS. 2019. Total Synthesis of the Bacterial Diisonitrile Chalkophore SF2768.
710 Org Lett 21:8731-8735.
711 36. Kalia NP, Singh S, Hards K, Cheung CY, Sviriaeva E, Banaei-Esfahani A, Aebersold R,
712 Berney M, Cook GM, Pethe K. 2023. M. tuberculosis relies on trace oxygen to maintain
713 energy homeostasis and survive in hypoxic environments. Cell Rep 42:112444.
714 37. Soma S, Latimer AJ, Chun H, Vicary AC, Timbalia SA, Boulet A, Rahn JJ, Chan SSL,
715 Leary SC, Kim BE, Gitlin JD, Gohil VM. 2018. Elesclomol restores mitochondrial function
716 in genetic models of copper deficiency. Proc Natl Acad Sci U S A 115:8161-8166.

717 38. Gotzke H, Kilisch M, Martinez-Carranza M, Sograte-Idrissi S, Rajavel A, Schlichthaerle
718 T, Engels N, Jungmann R, Stenmark P, Opazo F, Frey S. 2019. The ALFA-tag is a
719 highly versatile tool for nanobody-based bioscience applications. Nat Commun 10:4403.
720 39. Conradie F, Bagdasaryan TR, Borisov S, Howell P, Mikiashvili L, Ngubane N, Samoilova
721 A, Skornykova S, Tudor E, Variava E. 2022. Bedaquiline–pretomanid–linezolid regimens
722 for drug-resistant tuberculosis. New England Journal of Medicine 387:810-823.
723 40. Conradie F, Diacon AH, Ngubane N, Howell P, Everitt D, Crook AM, Mendel CM, Egizi
724 E, Moreira J, Timm J. 2020. Bedaquiline, pretomanid and linezolid for treatment of
725 extensively drug resistant, intolerant or non-responsive multidrug resistant pulmonary
726 tuberculosis. The New England Journal of Medicine 382:893.
727 41. de Jager VR, Dawson R, van Niekerk C, Hutchings J, Kim J, Vanker N, van der Merwe
728 L, Choi J, Nam K, Diacon AH. 2020. Telacebec (Q203), a new antituberculosis agent.
729 New England Journal of Medicine 382:1280-1281.
730 42. Beites T, O'Brien K, Tiwari D, Engelhart CA, Walters S, Andrews J, Yang HJ, Sutphen
731 ML, Weiner DM, Dayao EK, Zimmerman M, Prideaux B, Desai PV, Masquelin T, Via LE,
732 Dartois V, Boshoff HI, Barry CE, 3rd, Ehrt S, Schnappinger D. 2019. Plasticity of the
733 Mycobacterium tuberculosis respiratory chain and its impact on tuberculosis drug
734 development. Nat Commun 10:4970.
735 43. Cai Y, Jaecklein E, Mackenzie JS, Papavinasasundaram K, Olive AJ, Chen X, Steyn
736 AJC, Sassetti CM. 2021. Host immunity increases Mycobacterium tuberculosis reliance
737 on cytochrome bd oxidase. PLoS Pathog 17:e1008911.
738 44. Bhatt K, Machado H, Osorio NS, Sousa J, Cardoso F, Magalhaes C, Chen B, Chen M,
739 Kim J, Singh A, Ferreira CM, Castro AG, Torrado E, Jacobs WR, Jr., Bhatt A, Saraiva M.
740 2018. A Nonribosomal Peptide Synthase Gene Driving Virulence in Mycobacterium
741 tuberculosis. mSphere 3.
742 45. Botella H, Peyron P, Levillain F, Poincloux R, Poquet Y, Brandli I, Wang C, Tailleux L,
743 Tilleul S, Charriere GM, Waddell SJ, Foti M, Lugo-Villarino G, Gao Q, Maridonneau-
744 Parini I, Butcher PD, Castagnoli PR, Gicquel B, de Chastellier C, Neyrolles O. 2011.
745 Mycobacterial p(1)-type ATPases mediate resistance to zinc poisoning in human
746 macrophages. Cell Host Microbe 10:248-59.
747 46. Boudehen YM, Faucher M, Marechal X, Miras R, Rech J, Rombouts Y, Seneque O,
748 Wallat M, Demange P, Bouet JY, Saurel O, Catty P, Gutierrez C, Neyrolles O. 2022.
749 Mycobacterial resistance to zinc poisoning requires assembly of P-ATPase-containing
750 membrane metal efflux platforms. Nat Commun 13:4731.

751 47. Darwin KH. 2015. Mycobacterium tuberculosis and Copper: A Newly Appreciated
752 Defense against an Old Foe? J Biol Chem 290:18962-6.
753 48. Chen T-Y, Chen J, Ruszczycky MW, Hilovsky D, Hostetler T, Liu X, Zhou J, Chang W-c.
754 2024. Variation in Biosynthesis and Metal-Binding Properties of Isonitrile-Containing
755 Peptides Produced by Mycobacteria versus Streptomyces. ACS Catalysis 14:4975-
756 4983.
757 49. Shi L, Sohaskey C, Kana B, Dawes S, North R, Mizrahi V, Gennaro M. 2005. Changes
758 in energy metabolism of Mycobacterium tuberculosis in mouse lung and under in vitro
759 conditions affecting aerobic respiration. Proceedings of the National Academy of
760 Sciences of the United States of America 102:15629-15634.
761 50. Harikishore A, Mathiyazakan V, Pethe K, Grüber G. 2023. Novel targets and inhibitors of
762 the Mycobacterium tuberculosis cytochrome bd oxidase to foster anti-tuberculosis drug
763 discovery. Expert Opinion on Drug Discovery 18:917-927.
764 51. Andrews S. 2010. FastQC: a quality control tool for high throughput sequence data.
765 http://www.bioinformatics.babraham.ac.uk/projects/fastqc. Accessed
766 52. Li H, Handsaker B, Wysoker A, Fennell T, Ruan J, Homer N, Marth G, Abecasis G,
767 Durbin R. 2009. The Sequence Alignment/Map format and SAMtools. Bioinformatics
768 25:2078-9.
769 53. Li H, Durbin R. 2009. Fast and accurate short read alignment with Burrows-Wheeler
770 transform. Bioinformatics 25:1754-60.
771 54. Liao Y, Smyth GK, Shi W. 2014. featureCounts: an efficient general purpose program for
772 assigning sequence reads to genomic features. Bioinformatics 30:923-30.
773 55. Love MI, Huber W, Anders S. 2014. Moderated estimation of fold change and dispersion
774 for RNA-seq data with DESeq2. Genome Biol 15:550.
775 56. Kolde R. pheatmap, https://rdocumentation.org/packages/pheatmap/versions/1.0.12.
776 57. R Core Team R. 2013. R: A language and environment for statistical computing.
777
778

779 **Supplementary Materials**

780

781 Figures S1-S5

782

783 Supplementary Tables:

784 Table S1: strains used

785 Table S2: plasmids used

786 Table S3: RNA sequencing dataset

787

788 SI appendix 1: chemical synthesis methods